Carbon Balance and Management

METHODOLOGY

Open Access

The Greenhouse gas Observations of Biospheric and Local Emissions from the Upper sky (GOBLEU): a mission overview, instrument description, and results from the first flight

Hiroshi Suto[1*], Akihiko Kuze[1], Ayako Matsumoto[2], Tomohiro Oda[3,4,5], Shigetaka Mori[6], Yohsuke Miyashita[2], Chiharu Hoshino[1], Mayumi Shigetoh[1], Fumie Kataoka[7] and Yasuhiro Tsubakihara[2]

Abstract

Background The Greenhouse gas Observations of Biospheric and Local Emissions from the Upper sky (GOBLEU) is a new joint project by Japan Aerospace Exploration Agency (JAXA) and ANA HOLDING INC. (ANAHD), which operates ANA flights. GOBLEU aims to visualizes our climate mitigation effort progress in support of subnational climate mitigation by collecting greenhouse gas (GHG) data as well as relevant data for emissions (nitrous dioxide, NO_2) and removals (Solar-Induced Fluorescence, SIF) from regular passenger flights. We developed a luggage-sized instrument based on the space remote-sensing techniques that JAXA has developed for Japan's Greenhouse gas Observing SATellite (GOSAT). The instrument can be conveniently installed on a coach-class passenger seat without modifying the seat or the aircraft.

Results The first GOBLEU observation was made on the flight from the Tokyo Haneda Airport to the Fukuoka Airport, with only the NO_2 module activated. The collected high-spatial-resolution NO_2 data were compared to that from the TROPOspheric Monitoring Instrument (TROPOMI) satellite and surface NO_2 data from ground-based air quality monitoring stations. While GOBLEU and TROPOMI data shared the major concentration patterns largely driven by cities and large point sources, regardless of different observation times, we found fine-scale concentration pattern differences, which might be an indication of potential room for GOBLEU to bring in new emission information and thus is worth further examination. We also characterized the levels of NO_2 spatial correlation that change over time. The quickly degrading correlation level of GOBLEU and TROPOMI suggests a potentially significant impact of the time difference between CO_2 and NO_2 as an emission marker and, thus, the significance of co-located observations planned by future space missions.

*Correspondence:
Hiroshi Suto
suto.hiroshi@jaxa.jp

Full list of author information is available at the end of the article

Conclusions GOBLEU proposes aircraft-based, cost-effective, frequent monitoring of greenhouse emissions by GOBLEU instruments carried on regular passenger aircraft. Theoretically, the GOBLEU instrument can be installed and operated in most commercially used passenger aircraft without modifications. JAXA and ANAHD wish to promote the observation technique by expanding the observation coverage and partnership to other countries by enhancing international cooperation under the Paris Agreement.

Keywords Net zero, Paris accord, 1.5degree, Greenhouse gas, Climate monitoring, Climate mitigation, Global stocktake

Background

Under the Paris Agreement, countries submit their pledges toward the temperature goal in the form of Nationally Determined Contributions (NDCs), and their progress will be evaluated every five years from 2023 (Global Stocktake, GST). The first GST suggested that our climate mitigation effort is insufficient to achieve Paris agreement goal, and thus, we need further actions [1]. Science-based approaches are necessary to track and guide our actions to the second GST in 2028. The research community has explored the ways to utilize greenhouse gas (GHG) data collected from various observation platforms (e.g., ground, aircraft, and satellites) in order to support the evaluation at GST [2]. Over the past decade, GHG remote sensing has significantly advanced, matured, and started playing a key role in collecting GHG data for science [e.g., 3–12], and for climate mitigation monitoring applications [e.g., 13–15].

In 2020, the Japan Aerospace Exploration Agency (JAXA) and ANA HOLDINGS INC. (ANAHD) jointly launched a new project named Greenhouse gas Observations of Biospheric and Local Emissions from the Upper sky (GOBLEU) (https://www.eorc.jaxa.jp/GOSAT/ANAexp/index.html). In support of subnational climate mitigation efforts, GOBLEU collects GHG and other relevant data from regular passenger aircraft and visualizes our climate mitigation effort progress. GOBLEU aims to achieve the objective by combining JAXA's GHG remote-sensing technique and experiences built on the GOSAT mission and ANA's world-leading air passenger carrier capacity. Just a few years back, the COVID-19 pandemic hit the airline industry hard due to the travel restrictions implemented globally [16]. The number of passenger flights in 2020 dropped by 60% from 2019 [17]. Airlines have not carried passengers at full capacity for over two years, including the Olympic and Paralympic Games 2021 in Tokyo. However, GOBLEU turns " ghost " flight operations into action for climate monitoring and mitigation by carrying a GHG monitoring instrument on board passenger flights and contributing to sustainability.

JAXA and ANAHD have designed and developed an innovative carry-on size instrument suite that can be installed on two window seats and collects data through the cabin window, just like a passenger. The GOBLEU instruments are based on the same remote-sensing observation technique developed and used by the current state-of-the-art GHG observing GOSAT (2009-on, 3) and GOSAT-2 (2018-on, 6) satellites. The instrument suite is designed to collect carbon dioxide (CO_2) data as well as additional variables, such as nitrogen dioxide (NO_2) levels as a tracer of CO_2 from fuel combustion and solar-induced fluorescence (SIF) as an indicator of the plant production (carbon removals) of the terrestrial biosphere (e.g., forests and other vegetated areas) [18, 19]. This is expected to enhance the ability to monitor carbon emissions and removals from major key emission sectors and provide GHG information relevant to climate mitigation tracking at various decision making and climate action levels. Data to be collected by GOBLEU and the derived GHG information are complementary to common GHG information, such as emission inventories. These are typically developed and updated on a relatively low frequency (often annually) with high latency (more than a year or two). GOBLEU expects to provide timely GHG information by promptly collecting high-resolution GHG data and emission and removal estimates with greater information granularity. The high-spatial-resolution data should provide GHG information to stakeholders at different subnational levels (e.g., states/prefectures, cities, the private sectors, and citizens).

GOBLEU should also provide direct technical and scientific implications to the synergic use of remotely sensed GHG and AQ data that is planned by future space GHG observing missions, such as Japan's Global Observing SATellite for Greenhouse gases and Water cycle (GOSAT-GW; planned launch 2024) [20] and Europe's Copernicus Carbon Dioxide Monitoring mission (CO2M; planned launch 2026) [21]. As recent studies [22–26] demonstrated, simultaneously collecting CO_2 and NO_2 data should enhance our ability to quantify anthropogenic GHG emissions. However, it is important to note that the previous studies have been based on data from different satellite platforms based on certain spatial and temporal colocation criteria or a campaign flight.

The first GOBLEU proof of concept flight occurred on the 26th of October 2020 during the global COVID pandemic. This manuscript describes the instrument, the first flight, and the results. We also discuss the current challenges and limitations as well as our plans.

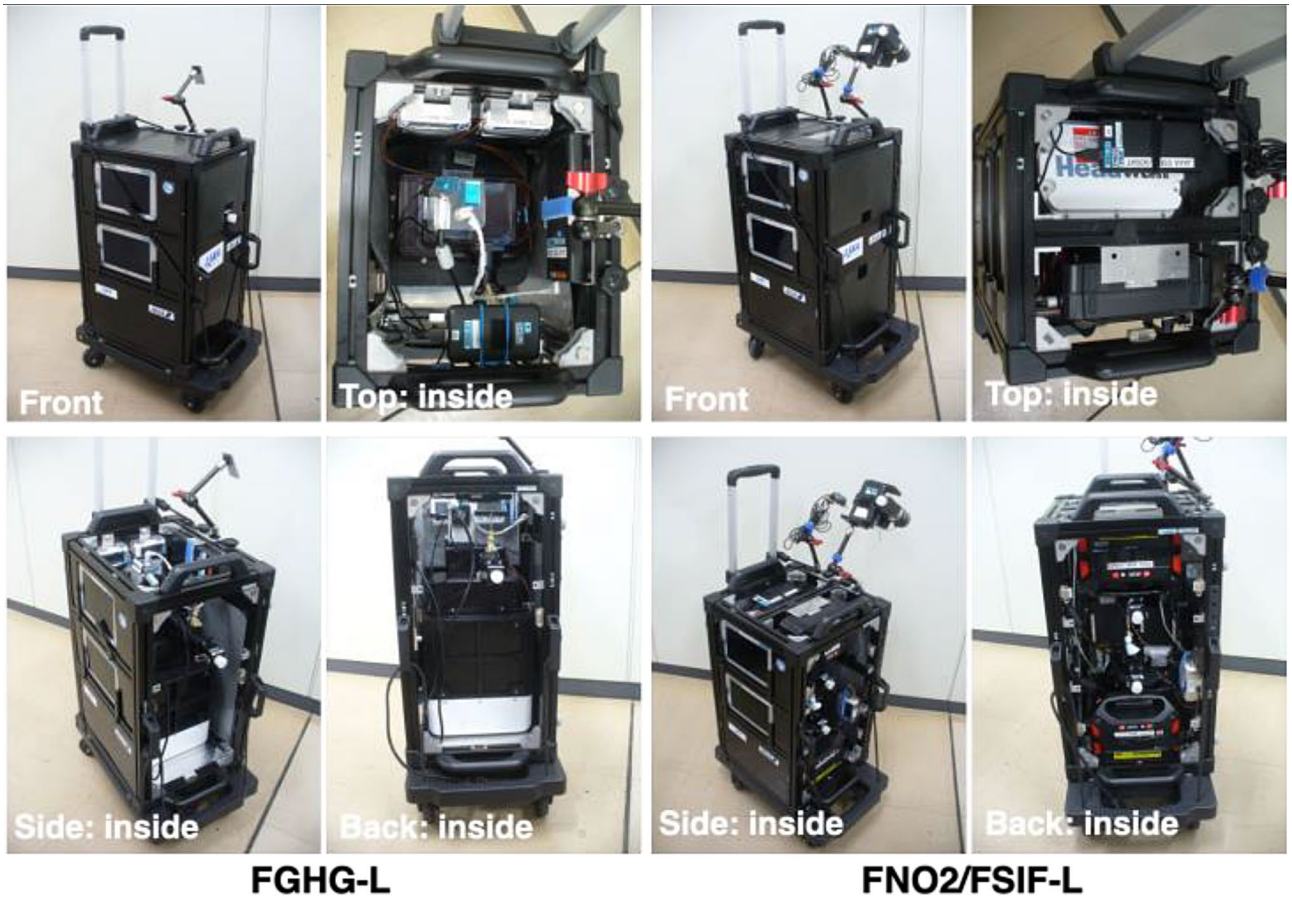

Fig. 1 The GOBLEU monitoring instrument suite. The instrument suite consists of two modules: GHG observation (left) and NO_2/SIF observation (right). These modules are connected by optical fiber from the window seat. The instrumental parameters, including the observation setting, differ between left-side and right-side seats. The instruments are labeled as "-L" or "-R" for their proper seat to avoid missetting

Table 1 A summary of instrument details

Instruments	FNO2	FSIF	FGHG
Spectral range	420–490 nm	670–780 nm	1560–1640nm
Spectral bands	2048	2048	640
Spectral sampling interval	0.03 nm	0.05 nm	0.17 nm
Spectral resolution (FWHM)	0.8 nm	0.17 nm	0.3 nm
Spatial pixels	2048	2048	512
Bundled spatial pixels	53		
Field of view	31°		
Instantaneous field of view	0.58°		
Spatial sampling interval (along-track)	0.5 s		

Methods

GOBLEU monitoring instrument suite

Figure 1 shows the GOBLEU monitoring instrument suite. Before the GOBLEU project launched, we evaluated the transmissivity of the cabin window using ASD FieldSpec4 (a wide-spectral range spectrometer). We confirmed that most cabin windows on ANA-operated aircraft transmit the reflected solar light spectra between 400 nm and 1650 nm sufficiently for the measurement, except for windows with an electronic shade. Given the spectral range, GOBLEU has chosen CO_2 as the main target GHG. The instrument suite consists of three in-house customized imaging (grating) spectrometers coupled with 53 arrays of bundled optical fibers: Fiber-coupled NO_2 imaging spectrometer (FNO2), Fiber-coupled SIF imaging spectrometer (FSIF), and Fiber-coupled Greenhouse gas imaging spectrometer (FGHG). Details of the spectrometers are summarized in Table 1. A common fore-optics relay is the solar light reflected on the Earth's surface through the bundled optical fibers. Three

instruments cover the spectral ranges in 420–490 nm for NO_2, 670–780 nm for SIF, and 1560–1640 nm for CO_2, with spectral sampling intervals of 0.03 nm, 0.05 nm, and 0.17 nm, respectively. These spectrometers are coupled with a 2-dimentional (2D)-CMOS camera (2048×2048) for NO_2 and SIF and an 2D-InGaAs camera (640×512) for CO_2 manufactured by Hamamatsu Photonics K.K. GOBLEU is a push broom hyperspectral imager, integrating spectroscopy and 2D-spatial mapping in one single system for each target species.

CO_2, NO_2, and SIF imaging spectrometers are packed in two carry-on luggage-sized boxes (one for NO_2 and SIF observation and one for CO_2 observation, 320 mm (W) x 380 mm (D) x 600 mm (H) per pack). They weigh less than 30 kg and collect high-spatial-resolution remote-sensing spectra of NO_2, SIF, and CO_2.

Like passengers, these " passenger " instrument boxes are mounted on seats also with seatbelts. Thus, no modifications to the aircraft are needed. In theory, these instrument suites can take a cabin seat on either side of the aircraft; however, we must switch the setting depending on the side of choice and optimize the coordination. To avoid the missetting, the instrument suites are labeled as "-L" for left-side use and "-R" for right-side use. Figure 1 shows the instrument models for left-side seats. The typical spectra observed by the imaging suites, presented in Fig. 1, are also plotted in Fig. 2.

The optical lens and optical fibers are made of quartz glass for wide-spectral coverage. Two packed instruments can be handily to mounted on a passenger economy (coach) class seat. The input optics, the passengers' "eye", combines a wide viewing lens and an inertial navigation unit, coupled with a Global Positioning System (GPS) signal receiver, to collect the solar radiation reflected by the Earth's surface and identify the starting locations.

In addition, during taxing before and after the observation flight, a mechanical shutter shields the lens, and the dark spectra are acquired for reference. While the cabin pressure and temperature of passenger aircraft are well controlled, localized temperature gradients around the instrument suites should be avoided. Circulators are installed for each instrument suite. Both navigation and spectra data are simultaneously logged on a laptop computer through a USB-3.0 connection, and the collected data can be monitored in flight.

All the electronic power for the electronic devices, including camera image acquisition, is supplied by a mobile Li-ion battery (Fujikura BA-155, 155 Wh). The battery capacity needs to be less than 160 Wh to be on board an aircraft, according to a regulation by Japan's

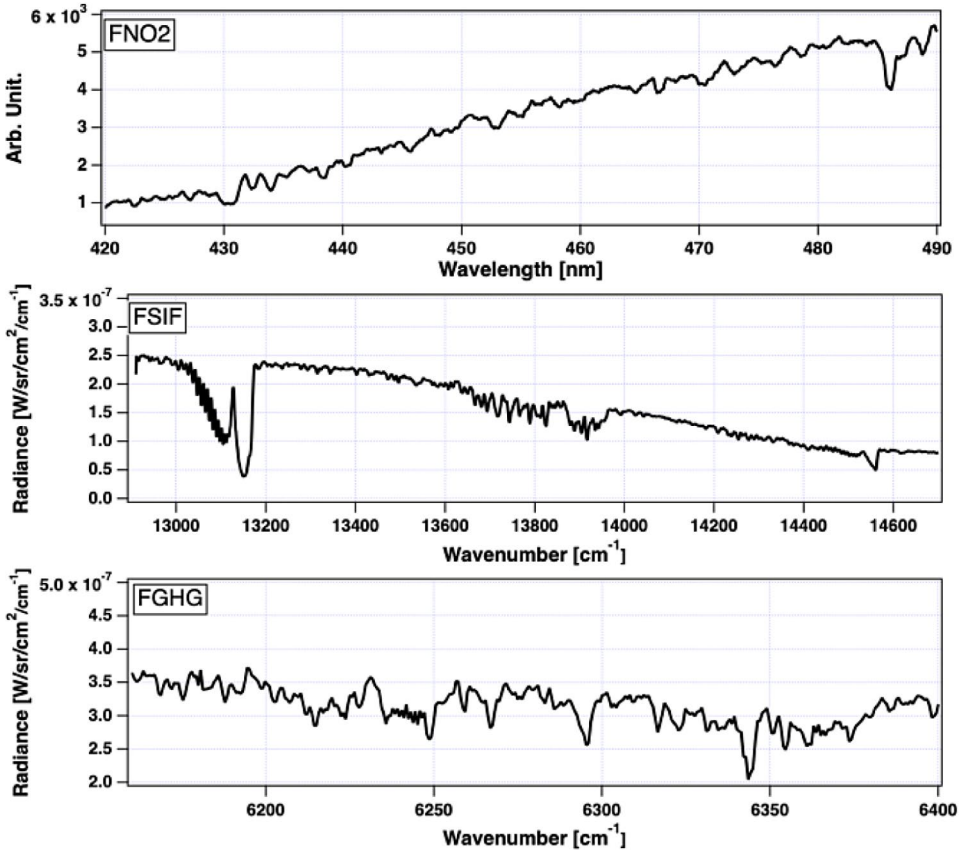

Fig. 2 The collected spectra by FNO2 (top), FSIF (middle), and FGHG (bottom) during a ground function test period

Ministry of Land, Infrastructure, Transport and Tourism (MLIT). The power supply is installed in carry-on luggage-sized boxes, and this configuration is permissible on ANA flights. A single battery with the current observation configuration allows continuous NO_2, SIF, and CO_2 observation for at least three hours. For round-trip observation, these batteries can be switched with fully recharged packs at the airport, allowing an additional three hours of observations.

The retrieval principles

To retrieving NO_2, SIF, and CO_2, the differential optical absorption spectroscopy (DOAS) technique [27], the iterative maximum a posteriori differential optical absorption spectroscopy (IMAP-DOAS) technique [28] and full physics retrieval technique [e.g. 29–37] are planned to apply, respectively.

The NO_2 absorption lines allocated between 420 and 490 nm are applied DOAS spectral fit. To process the DOAS fit for NO_2 retrieval from GOBLEU, the QDOAS software is optimized for GOBELU analysis [38]. The detail of NO_2 retrieval setting and data analysis are described in results section.

Solar induced Chlorophyll Fluorescence (SIF) is emitted between 600 nm and 900 nm with the peak at 685 nm [39]. To observe the SIF with remote-sensing, the isolated Fraunhofer lines (absorption features in the solar atmosphere) are used to retrieve the fluorescence emission intensity from O2 A-band observed by GOSAT [40–44]. In addition, SIF is retrieved from GOME-2, TROPOMI [45–47] both O2 A-band and B-band. To cover the isolated Fraunhofer lines allocated both O2 A- and B-bands for SIF retrieval, our instrument cover between 670 and 780 nm with 0.05 nm spectral sampling interval. SIF emission intensity from the collected GOBLEU spectra is planned to retrieval by optimizing the iterative maximum a posteriori differential optical absorption spectroscopy (IMAP-DOAS) technique [28] both O2 A- and B- bands regions.

In the case of space-based CO_2 observation, 1.6 μm (weak CO_2 absorption spectra) and 2.0 μm (strong CO_2 absorption spectra) of CO_2 bands are used as CO_2 retrieval channels among GOSAT [29–35], GOSAT-2 [36, 37], OCO-2 [48] and OCO-3 [48]. These retrievals are coupled with strong and week CO_2 channels and O2A channels to detect the effective optical path length. The transmittance of cabin window only allows to transmit week CO_2 spectra. The CO_2 retrieval from GOBLEU flight will be performed with full physics algorithm, its constructed with the simultaneous spectral fit between the observed week CO_2, O_2 A-band spectra and theoretical radiative transfer calculation. Additionally, IMAP-DOAS for CO_2 [49] is also considered to first processing of CO_2 enhancement in the region of interest.

Observation pattern

The passenger's eye views the slant nadir through the cabin window, where the observation viewing angle is managed around +65 ° from the nadir to avoid the vignetting of the solar light reflecting the Earth's surface and stray light from the cabin window and its frame. The pictures of GOBLEU imaging spectrometer suites mounted on the seat of an ANA aircraft are presented in Fig. 3. This configuration can provide wide spatial coverage. From one side of the aircraft (as shown in Fig. 4), the spatial coverage is around 50 km with an 11 km flight altitude and +65 ° viewing angle. It directly depends on flight altitude and viewing angles. The spatial coverage

Fig. 3 The GOBLEU instrument suite onboard the ANA aircraft. The instruments are seated on cabin seats (top left panel), targeting the input optics to slant-view thorough the cabin window (top right panel)

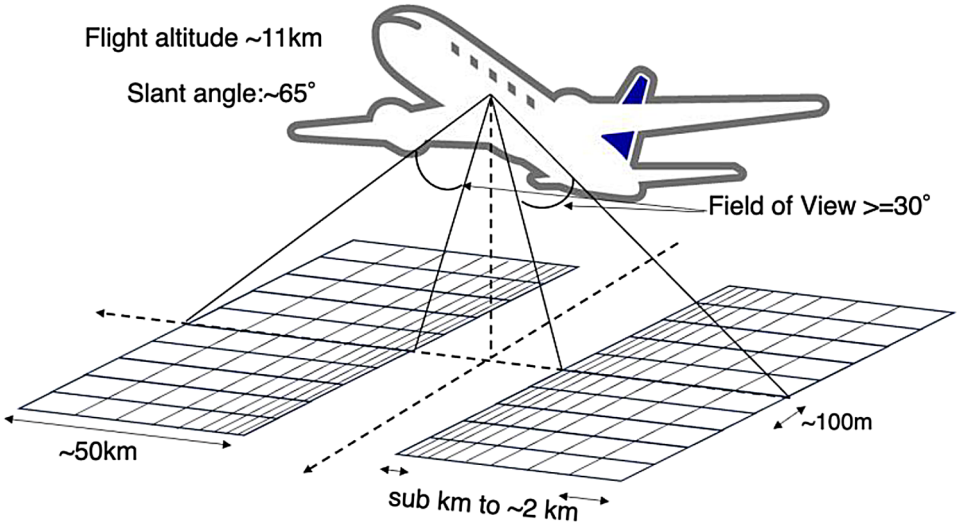

Fig. 4 The GOBLEU observation configuration. "New passenger" (Monitoring instruments) onboard ANA passenger flights and slant-viewing to detect changes in NO_2, SIF, and CO_2 levels over the surface using cabin seats. A typical sampling distance in along-track is 100 m with 50 km across-track coverage. In the double-side case, the coverage is up to 100 km. The sampling size for across-track direction depends on the viewing angle from the aircraft, and it varies from sub-km to 2 km

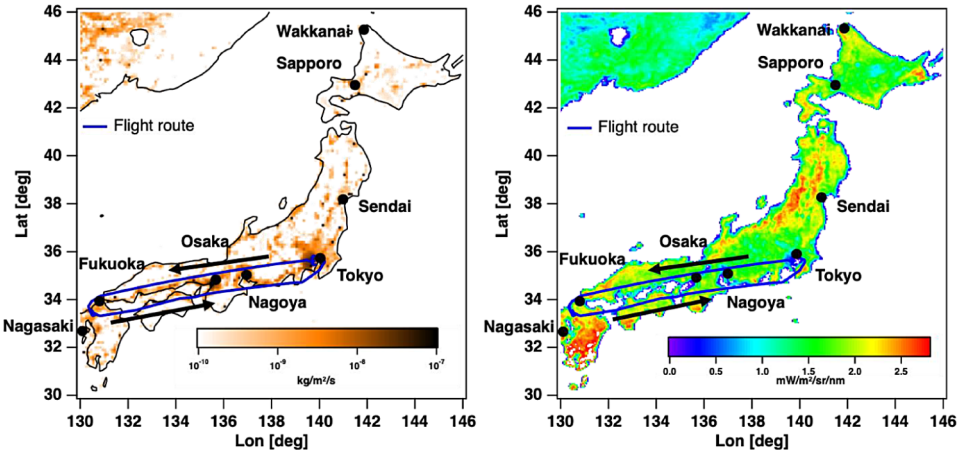

Fig. 5 The observation flight route with an EDGAR CO_2 emission map (left) and a TROPOMI SIF intensity map (right). Flight routes cover Tokyo, Osaka, Nagoya, Fukuoka, Sendai, and Sapporo in Japan and industrial area between Tokyo to Fukuoka

can be easily doubled by expanding to two-side (right and left side of the aircraft) observation with additional carry-on equipment. The ground sampling distance (GSD) is 100 m (along-track) by sub km (across-track) assuming a typical altitude of 11 km a. g. l., ground speed of 200 m/s and integration time of 500 milli-seconds. This configuration will support an increase in monitoring frequency and spatial coverage. In the case of double-sides observation, the coverage for across-track is up to around 100 km with 100 m along-track spatial resolution, which is ten times higher than current satellites.

Flight route plan

The ANA flight nationwide route network that connects Japan's megacities should allow our observations to focus on collecting data over those intense local emission areas where current satellites have had a challenge to collect data. As described earlier, our operation can be extended to three hours without replacing a battery. We can select any direction from Tokyo Haneda Airport in this time frame. The longest leg is northward from Tokyo Haneda Airport to Hokkaido Wakkanai Airport, which takes three hours. Southward, a 2.5-hour flight from Tokyo Haneda Airport to Kyushu-Nagasaki Airport is allowed. These flights cover the major Japanese megacities and large industrial areas. The main observation route, from Tokyo Haneda Airport to Fukuoka Airport, is illustrated in Fig. 5 coupled with the Emissions Database for Global Atmospheric Research (EDGAR) CO_2 [50–52] emission map (left) and the one-year integrated TROPOMI SIF

Table 2 A summary of the first GOBLEU flight

Date	2020-10-26
Time	01:02–02:22 UTC and LT10:02–11:22
Location	From Tokyo Haneda Airport to Fukuoka Airport
Range	From 33.5ºN 139.8 ºW to 33.6ºN 130.4ºW
Aircraft (Aircraft Registration)	Boeing 767 – 300 (JA607A)
Flight Number	NH247
Observation Target	NO_2
Solar zenith angle range	47.4º to 53.8º

Fig. 6 Carry-on instrument with operator. The picture was taken just before the security gate of Haneda Airport Terminal 2. The instrument is brought as carry-on luggage for the operator

intensity [53] (right). The left panel in Fig. 5 illustrates the Tokyo Haneda to Kyusyu Fukuoka flight route and CO_2 emission strength based on EDGAR CO_2. These routes cover Japanese megacities such as Tokyo (pop: 140 M), Osaka (pop: 88.2 M), Nagoya (pop: 22.9 M), Fukuoka (pop: 15.4 M), Sendai (pop: 10.8 M), and Sapporo (pop: 19.5 M). Also, the major industrial areas in Japan are often located in coastal areas, such as Tokyo Bay, Nagoya Bay, Osaka Bay, and Setouchi Bay. Regular passenger flights also cover these areas. Normally, it takes two hours from Tokyo Haneda Airport to Fukuoka Airport (the southern mega city in Japan). The two-hour flight allowed us to collect soundings every 0.5 s (around 0.8 million observations per side in two-hour flight; 53 across-track x 2 images/sec x 2 h) from 130°E to 140°E in longitude and 33.5°N to 36°N in latitude (about a 900 km travel distance).

Results

The first GOBLEU flight and data processing

On the 26th of October 2020, during the COVID-19 pandemic, the GOBLEU monitoring suite began its first trip from the Tokyo Haneda Airport to the Fukuoka Airport with an ANA regular flight (NH247). A summary of the first flight is shown in Table 2. This flight aimed to realize our observation concept; thus, only the NO_2 module was activated. The main objective was to monitor NO_2, CO_2, and SIF via the cabin window using remote-sensing technology and operation on board a passenger aircraft. To focus on the proof of our observation concept (e.g., performed by one person for one instrument), the first observation test was performed using the NO_2 instrument only with the minimum number of support staff. It also aimed to reduce the risk of Coronavirus infection during the COVID-19 pandemic.

The prototype instrument, with the same imaging spectrometer and input optics of the complete package shown in Fig. 1 but mounted on prototype packaging, was treated by an operator as carry-on luggage from the laboratory to Tokyo Haneda Airport (see Fig. 6). After passing through the security inspection including X-ray testing, the instrument was ready for the on-board commercial flight. The "passenger" instrument has been granted permission to be installed on the aircraft after conducting thorough radio interference checks and confirming with the airline that it will not cause any interference. With two pieces of carry-on luggage, any domestic observation flight from the Tokyo Haneda airport (central Japan) can be selected.

To secure the preparation time for the instrument on the cabin seat, we were preboarded ten minutes before regular boarding in the first trial. Then, the instrument was fixed with a seatbelt, as would be a typical passenger. As expected, the aircraft departed on time and took off smoothly. Once the captain turned the seatbelt sign off, we inspected the instrument and confirmed that there was no damage due to takeoff. During the flight, the operator constantly checked the computer display, which indicated two spectra in one second, real-time aircraft position and attitude, and file storage status. Also, the operator noted the weather conditions at several key locations, such as megacities and industrial areas.

The weather was fine for the first flight. The operator could observe the ground over Nagoya, Osaka, and the industrial area over Setouchi Bay. After 1.5 h from takeoff from the Tokyo Haneda airport, the aircraft landed at Fukuoka airport. Since the GOBLEU package was firmly mounted in the cabin seat, we did not observe any damage to the package during the landing. At Fukuoka Airport, the instrument suite was "relaxed" and unmounted and left the aircraft as the last passenger from the flight.

The collected spectra were analyzed by using the differential optical absorption spectroscopy (DOAS) technique to retrieve NO_2 data. The DOAS spectral fit was done for the 430–460 nm, which is optimal for NO_2 retrieval from GOBLEU using the QDOAS software.

In this spectral fit, the differential slant column densities (*dSCD*) are retrieved with a reference for DOAS

analysis, which spectra acquired over the rural area (no emission sources). The retrieved slant column density of NO_2 was converted to the vertical column density of NO_2 to consider the airmass factor (*AMF*)

Based on the visual inspection of simultaneously acquired visible camera images by GoPro 8, the highly cloud contaminated areas and the optimal reference area (no emission sources area) are identified. NO_2 absorption cross sections were subsequently fitted to the differential optical depth as well as O_2-O_2, H_2O, O_3, the pseudo ring spectrum interjacences. Spectrally slowly varying signatures were accounted for including a 3rd order polynomial in the fit. The spectral calibration is also conducted in QDOAS processing coupling with a high-resolution solar spectrum, implemented in QDOAS [54]. As for the instrumental line shape function, the error function, which is based on the convoluted box car and gauss function, is selected for this analysis.

The AMF is defined as the ratio between slant and vertical column of a trace gases. The AMF inferred from the radiative transfer model with geographic and atmospheric model parameters. In this study, the linearized discrete ordinate radiative transfer model: LIDORT [55] are employed with the climatological NO_2 profile, which provided from chemical transportation model results of the Tropospheric Chemistry reanalysis version 2 (TCR-2) database [56], surface albedo was set to the monthly climatology data of Lambertian-equivalent reflectivity (LER) derived from TROPOMI [57]. For the aerosol, Aerosol optical thickness (AOT) at 500 nm is applied the constant value of 0.21 coupled with gauss distribution model at1.5 km peak height. For other parameters such as O_3 vertical profile are used US standard atmosphere.

Through the optimal fitting by QDOAS, the $NO_2 dSCD_{obs}$, which is the difference between SCD_{obs} from the observation spectra and SCD_{ref} from the reference spectra, is derived and express the formulation in Eq. (1).

$$dSCD_{obs} = SCD_{obs} - SCD_{ref} \tag{1}$$

To deriving the vertical column density (VCD) of NO_2, the estimated $dSCD_{obs}$ are converted to VCD_{obs} coupled with AMF both observation (AMF_{obs}) and reference scene (AMF_{ref}), and the reference of vertical column density (VCD_{ref}) by applying the Eq. (2).

$$VCD_{obs} = \frac{dSCD_{obs} + VCD_{ref} \times AMF_{ref}}{AMF_{obs}} \tag{2}$$

The model parameters used AMF in the calculation, such as surface albedo, vertical profiles of trace gases including NO_2 and the aerosol scenario were kept constant throughout all observation points. These AMF calculations are conducted for each observation pixels both reference and target.

In this study, areas around 137.6$_\circ$ of longitude and 35.0$_\circ$ of latitude are selected as reference area and 1.35×10^{15} molec/cm^2 is assumed as VCD_{ref} reference concentration, which was determined using climatological NO_2 dataset based on monthly averaged TROPOMI observation data [58]. The differential approach cancels out the stratospheric NO_2 concentration to the signal, making the measurements only sensitive to tropospheric absorption, under the assumption that the stratospheric NO_2 filed has a negligible spatial and temporal variability during the time between the aquation of the reference spectrum and the measurements.

The error in the retrieved $NO_2 VCD_{obs}$ originates from uncertainties in the calculated $dSCD_{obs}$, SCD_{ref}, and AMF_{obs}. One assumes that the contributing uncertainties are sufficiently uncorrelated as they arise from nearly independent steps. Base on Eq. (1), the error of the $NO_2 VCD_{obs}$ retrieval algorithm can be quantified based on the following error propagation method [59]:

$$\sigma_{VCD} = \sqrt{\left(\frac{\sigma_{dSCD_{obs}}}{AMF_{obs}}\right)^2 + \left(\frac{\sigma_{dSCD_{ref}}}{AMF_{ref}}\right)^2 + \left(\frac{SCD_{obs} \times \sigma_{AMF_{obs}}}{AMF_{obs}^2}\right)^2} \tag{3}$$

To estimate a typical σ_{VCD}, Eq. (3) is considered with our flight data. The error in the DOAS fit, $\sigma_{dSCD_{obs}}$, is a direct output of QDOAS for each fit. In parallel, AMF_{obs} is calculated for each observation point coupled with modeled parameters. For the analysis areas including Nagoya and Osaka, the first term in the error estimation equation is calculated as 4.8×10^{15} molec/cm^2. (only in blanket in the first term.)

The second error term originates from the estimation of the NO_2 residual amount in the reference spectra ($\sigma_{dSCD_{ref}}$), which is determined as the standard deviation of reference observations fits. In this assumption, the second term is calculated as 5.9×10^{15} molec/cm^2. The calculated third term ($\sigma_{AMF_{obs}}$) has to be estimated based on the variation of modeled parameters.

It is too important to take the sensitivity of various parameter to AMF into account; however, it is beyond the scope of this study. Thus, the reference values, which were reported by [59], are applied in this estimation. In the literature, the relative error of $\sigma_{AMF_{obs}}$ was based on" Heavily polluted" condition in [59]. In this case, $\sigma_{AMF_{obs}}$ is assumed to be 0.6. To apply this assumption, the third term in the bracket is 6.8×10^{15} molec/cm^2. Finally, a typical σ_{VCD} was estimated to be 1.0×10^{16} molec/cm^2.

As shown in the following sections, we compared the retrieved NO_2 results with other data, such as satellite NO_2, a gridded emission inventory and ground-based in-situ observations.

The observed NO_2 at a glance

Figure 7 shows the collected first high-definition NO_2 map (Fig. 7a) showed good spatial pattern correspondence between both NO_2 data collected by the state-of-the-art satellite NO_2 instrument TROPOspheric Monitoring Instrument (TROPOMI) [60, 61] (Fig. 7b) and a high-resolution (1 km) gridded NO_X total emission estimates (Fig. 7c) developed by the Ministry of the Environment (MOE) (hereafter, MOEJ) [62], notably at megacities, such as Nagoya (pop: 7.5 M) and Osaka (pop: 8.8 M). The observation duration for these areas is around 30 min for GOBLEU and less than 1 min for

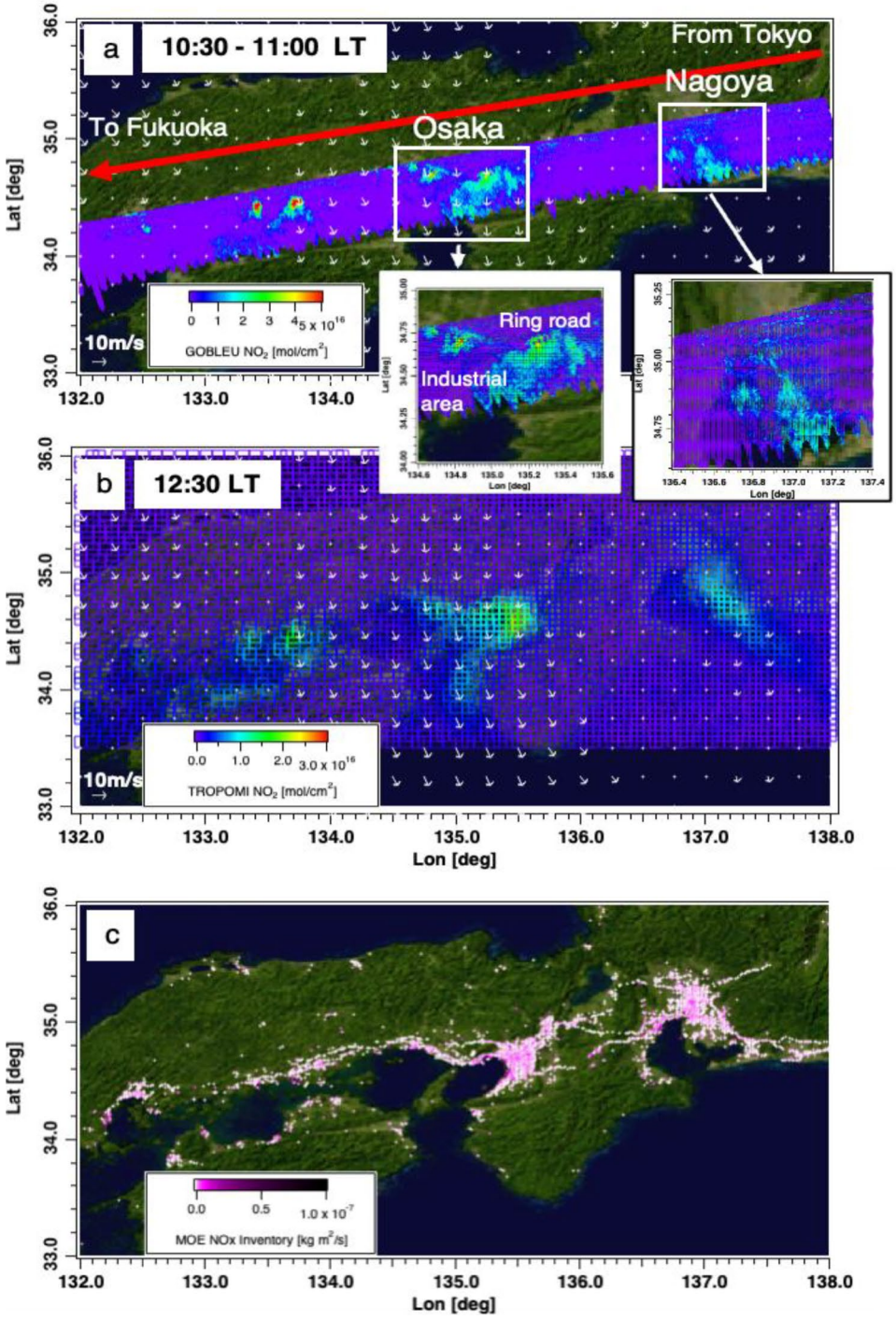

Fig. 7 NO_2 data collected during the first GOBLEU flight between Tokyo Haneda Airport and Fukuoka Airport (**a**) and from TROPOMI (**b**). The bottom panel (**c**) shows 1 km x 1 km total NOx emission values from the MOE inventory. The white arrows present the wind vector: GOBLEU for UT 10:00 and TROPOMI NO_2 for UT 12:00, respectively

TROPOMI. The white arrows present the wind vector taken from the ERA5 hourly wind dataset (GOBLEU for UT 10:00 and TROPOMI NO_2 for UT 12:00) [58, 63]. The map depicts the spatial pattern of NO_2 over the two megacities. In addition, the emissions from industrial areas are also clearly captured. The general spatial pattern is consistent with what TROPOMI satellite NO_2 observations captured approximately two hours after the GOBLEU flight.

GOBLEU and TROPOMI NO_2 spatial patterns are compared. Two NO_2 datasets (34°-37°in latitude and 132°-138°in longitude) were binned at a 0.05° and averaged. The values were finally aggregated latitudinally. The GOBLEU NO_2 map (aggregated mean in 0.05° longitudinal range, see Fig. 8) also showed good spatial correspondence with NO_2 data collected by TROPOMI (aggregated mean in 0.05° longitude range). While the observations were taken two hours apart, GOBLEU and TROPOMI NO_2 data shared major longitudinal spatial patterns peaking at megacity locations. It is important to note that GOBLEU data show more spatial features in the NO_2 field that seem to be co-located with large CO_2 sources of emission indicated by the EDGAR CO_2 inventory [50–52]. EDGAR CO_2 inventory data aggregated mean in the 0.1° longitudinal range is also plotted in Fig. 8.

The NO_2 spatial patterns over megacities

Looking closely at Nagoya and Osaka, the two maps showed different fine-scale spatial patterns. Figure 9 shows GOBLEU NO_2 aggregated to 0.005° x 0.005° and TROPOMI NO_2 aggregated in 0.05° x 0.05° with EDGAR CO_2 aggregated in 0.1° x 0.1°. The GOBLEU NO_2 map also depicts the point-wise intense NO_2 concentration, which collocated with the power generation facilities. The differences are unsurprising because two observations were taken at different local times (10:30 for Nagoya and10:45 for Osaka). The observed NO_2 concentration with different time presents the different concentration due to the diurnal cycles in emission and NOx-chemistry [64] as well as the wind magnitude/direction changes. However, they suggest the potential impact of observation time difference on the NO_2's performance as a marker for CO_2 emissions and highlight the significant benefit of simultaneous CO_2 and NO_2 observations for accurately estimating CO_2 emissions. Even a few hours' difference in observation time (which we see in previous studies) could significantly impact our ability to estimate CO_2 emissions using an NO_2 marker. In addition, the high-resolution observation should help capture the activity level emissions signatures. GOBLEU provides 10 or 20 times finer spatial structures of NO_2 concentrations than that of TROPOMI and the EDGAR inventory.

The spatial correspondence between GOBLEU and TROPOMI was further examined using the 0.05° aggregated data (Fig. 10). The difference could be attributable to the NOx-chemical process, wind speed and direction for NO_2 transportation, and diurnal emission changes of NO_2 due to the two-hour observation time difference, regardless of the potential contributing factors. The comparison shows that NO_2 concentration derived from GOBELU is almost similar range with that of well validated TROPOMI NO_2.

Temporal correlation of NO_2

GOBLEU NO_2 data's performance as a CO_2 emission marker was further examined by looking at spatial correlation with hourly NO_2 data from ground-based monitoring sites (https://soramame.env.go.jp/station), acknowledging known challenges (see Fig. 11). Hourly data from 136 ground stations in Nagoya and 251 ground stations in Osaka are used for this analysis. These stations are designed to monitor major local emission sources within the cities, such as traffic and industries, mainly for air quality monitoring purposes. The correlation with

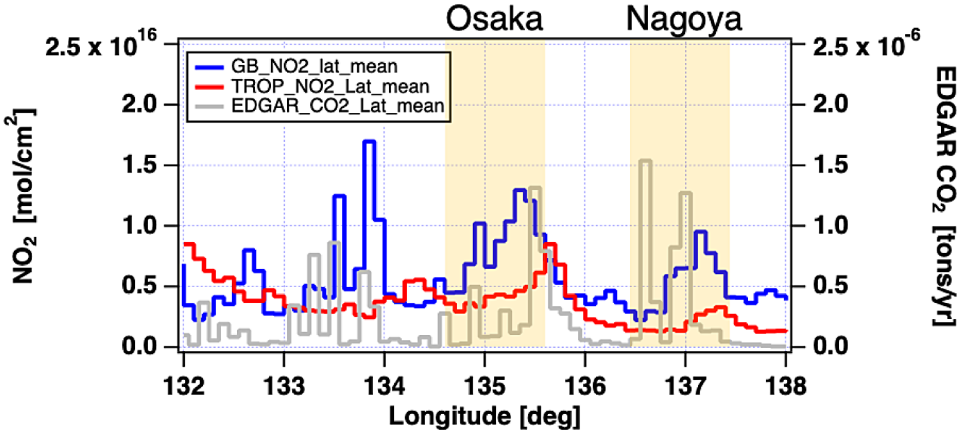

Fig. 8 0.05° latitudinally averaged NO_2 distribution of both GOBLEU (GB in blue) and TROPOMI (TROP in red) with EDGAR CO_2 inventory (Gray). Yellow shading area indicates megacities' longitudinal range. The Nagoya and the Osaka area are shaded

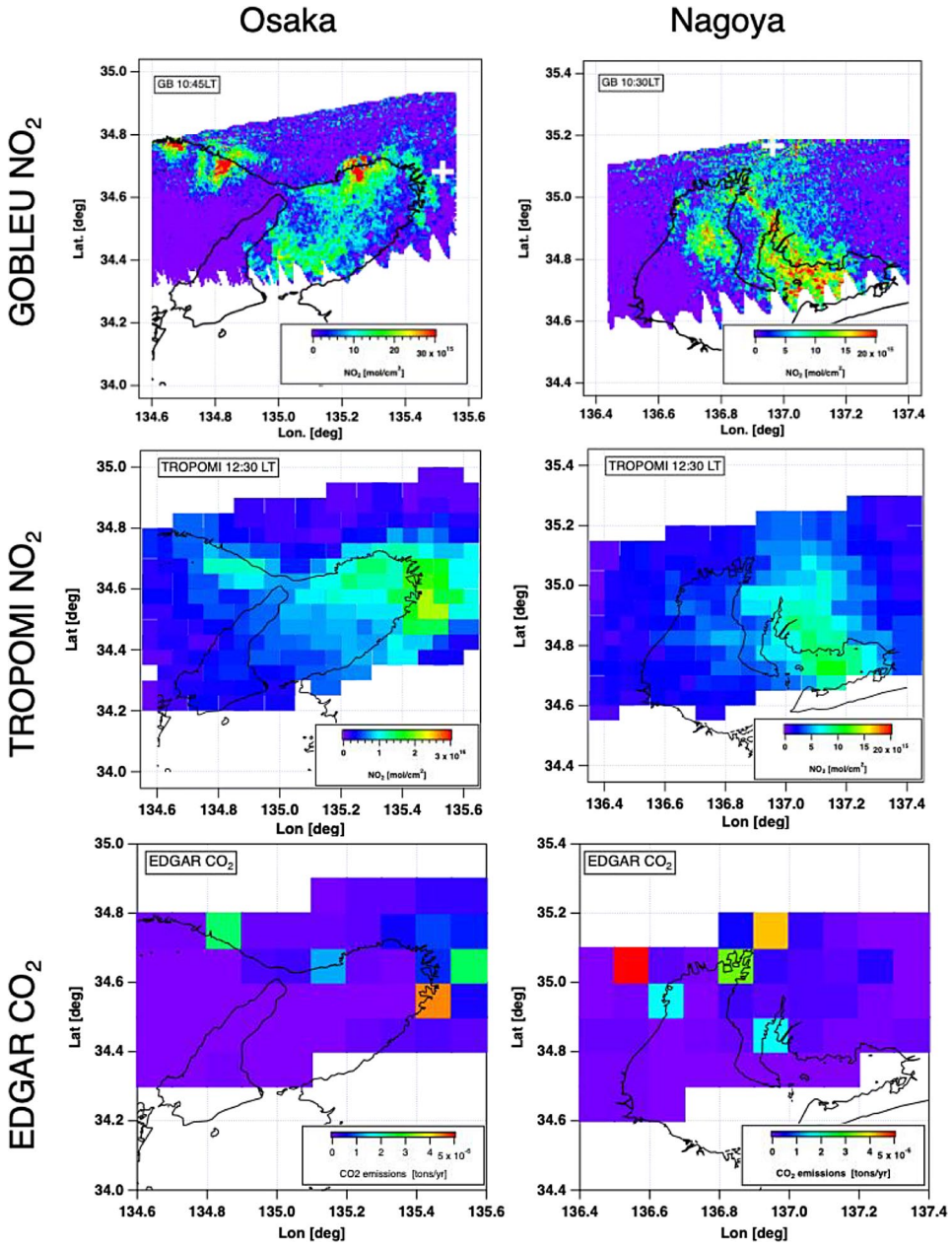

Fig. 9 NO_2 spatial patterns observed from GOBLEU (top) and TROPOMI (middle) during the first flight over Osaka (left) and Nagoya (right) during one flight. The boom row shows the spatial distributions of CO_2 emissions from the EDGAR inventory. Note that the local times for GOBLEU and TROPOMI are not the same. While the two remotely sensed NO_2 data share major spatial patterns, GOBLEU data captured fine-scale emission hot spots that might be diluted in TROPOMI data due to the spatial resolution

these observational data should be able to evaluate the sensitivity of the remotely sensed data to local emissions.

As expected, we found that GOBLEU's observations showed the best correlation at their local time (10:30 for Nagoya and 10:45 for Osaka). The level of the correlation went down significantly with time. Interestingly, while TROPOMI's correlations with the ground-based data peaked at the observation time (12:30 JST) for Nagoya, the Osaka case showed two correlation peaks in the morning (10 a.m. local time) and afternoon (2 p.m. local time). While GOBLEU and TROPOMI share the basic remote-sensing principle, GOBLEU captures NO_2 changes at the surface significantly better than TROPOMI. This is a caution for estimating emissions at a particular time of the day rather than obtaining an average emission over a certain period, using NO_2 as an emission marker. This analysis only loosely examined the skill at representing spatial patterns of potential CO_2 emissions. Accurately deriving emissions using these markers

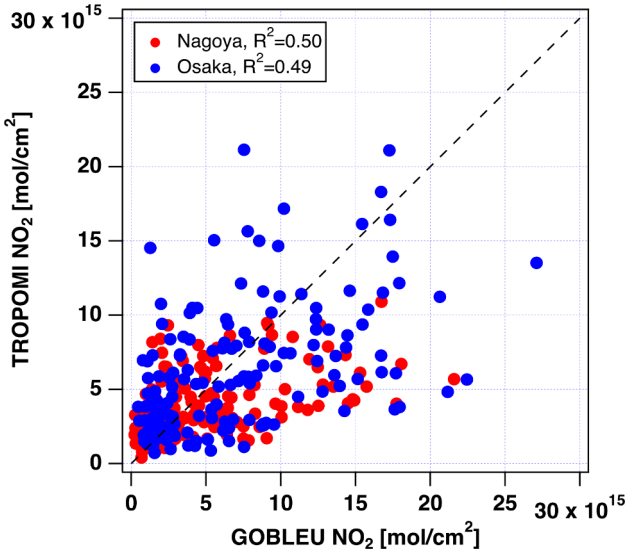

Fig. 10 Comparison of GOBLEU NO_2 and TROPOMI NO_2 in Nagoya (red filled circle) and Osaka (blue filled circle). The dotted lines represent the 1:1 line. The range of variation between GOBLEU and TROPOMI is similar but GOBLEU NO_2 present a higher concentration than that of TROPOMI. It seems that GOBLEU has highly sensitivity for local emission changes due to higher spatial resolution than that of TROPOMI

is yet another major challenge due to meteorology and chemistry.

Discussions

The first proof of concept flight with a NO_2 prototype instrument was successfully carried out. We proved and confirmed that our instrument collects science-quality useful spectra through the cabin window without modifying the aircraft. The airborne remote-sensing observation collects denser and finer spatial resolution GHG because the flight altitude of passenger aircraft (~ 11 km) is 1/60 of the current satellites (666 km) [3]. The follow-on instruments, a complete package of NO_2, SIF, and CO_2 modules, will be onboard both sides of the aircraft after the instrumental preparation and inspection. GOBLEU will simultaneously observe CO_2 and SIF, in other words, the emission and removal makers. The SIF information as an indicator for an activity level of removals is informative to improve our knowledge of biospheric removals and provide this information.

We also plan to perform extensive evaluation and validation of the collected data using the upper-looking data

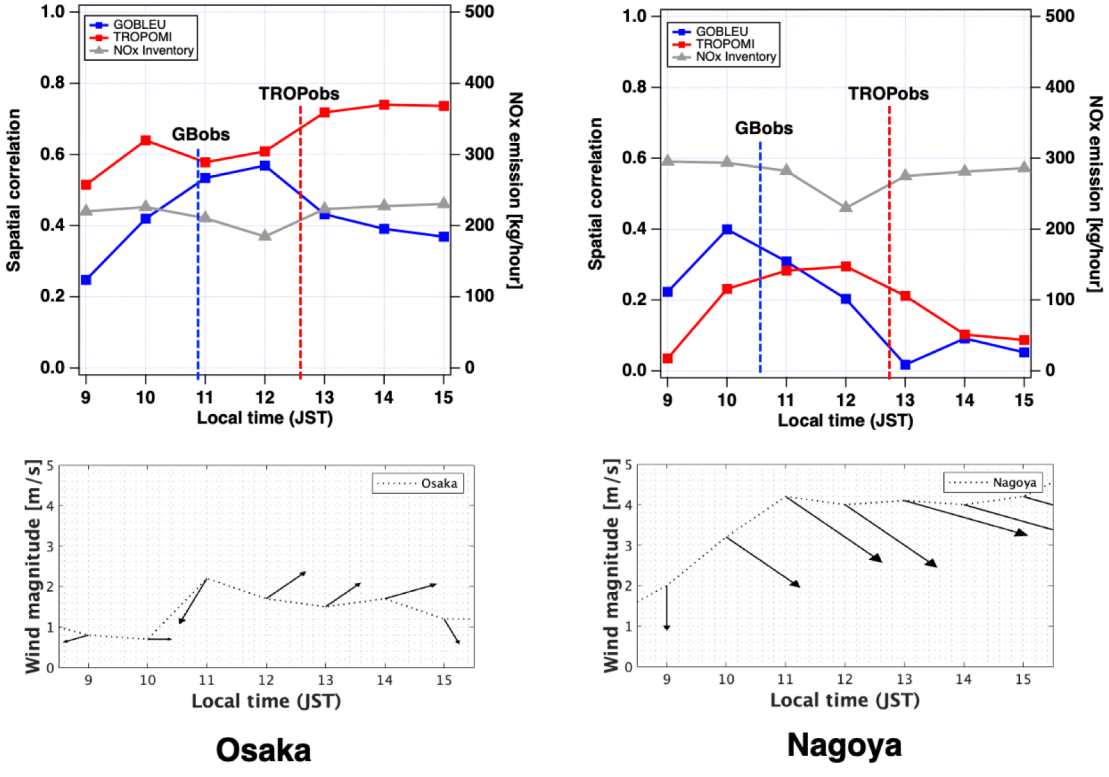

Fig. 11 Correlation analysis using remotely sensed NO_2 data from GOBLEU (GB in blue), TROPOMI (TROP in red), and hourly surface NO_2 data. The spatial correlation of remotely sensed and surface NO_2 was calculated over Osaka (top left) and Nagoya (top right) as a metric to characterize spatial patterns of two remotely sensed NO_2 levels. Hourly changed wind magnitude and direction are plotted in bottom panels. The vertical dotted lines indicate the local observation times for GOBLEU (blue) and TROPOMI (red). The gray line shows hourly NOx emission estimates taken from a gridded inventory developed by MOEJ. The correlation tends to be higher near the local observation times for GOBLEU and TROPOMI; however, the two remotely sensed NO_2 data collected roughly 1.5–2 h apart clearly showed a different correlation with the surface NO_2 over time. This suggests the significance of collocated NO_2 observations. The GOBLEU case showed much larger changes, which might be attributed to the higher spatial resolution of the data compared to TROPOMI

collected by the Total Carbon Column Observing Network (TCCON) [65] and Collaborative Carbon Column Observing Network (COCCON) [66]. These observations are based on the sun-directed ground-based spectrometer. As for NO_2, JAXA also prepared a ground-based instrument, PANDORA [67], for NO_2 validation. In the future, we will coordinate the validation campaign for our datasets to set the ground-based instrument under the flight route.

Our GOBLEU observation plans to prototype the synergistic use of CO_2 and NO_2 data and improve anthropogenic emission estimates. By using the correlation between CO_2 concentration and SIF intensity, GOBLEU also aims to estimate the carbon removals in the surrounding megacity area by the terrestrial biosphere. By observing emissions and removals, GOBLEU aims to collect actionable data for monitoring emissions from dominant source sectors, such as local traffic and industries, within cities and the removal impacts by the terrestrial biosphere. By visualizing the emission strength and reduction impact by utilizing new emission reduction technologies, our mitigation effort will be clearly depicted on the map. As also described in the results section, GOBLEU data has fine spatial resolution and is more detailed than that of state-of-the-art spaceborne imaging spectrometer instruments such as TROPOMI, OCO-3, and new geostationary air quality instruments: Geostationary Environment Monitoring Spectrometer (GEMS) [68]. Then, GOBLEU data can potentially validate these spaceborne datasets with finer spatial resolution data. Figure 12 presents the spatial distribution comparison between GOBLEU, TROPOMI, and OCO-3. GOBLEU and TROPOMI data are aggregated in 0.005° x 0.005°, in 0.05° x 0.05°, respectively. OCO-3 has a 1.29 km x 2.25 km spatial resolution. Comparing these plots, GOBLEU data depict the local pattern of NO_2 concentration.

While aircraft-based data are unique and valuable for GHG research [24], it is often challenging to increase data volume due to the cost. Our observations can be performed with two economy seats for instruments, the same as regular passengers. Taking a charter flight instead of a regular passenger flight increase the cost of one-flight up to several times. For example, two hours research flight could cost 2.4 K USD [https://www.jsforum.or.jp/other/zerog/]. Also, every day, passenger flights are scheduled to fly from one city to another, and seats can greatly increase the chance for observability. These situations are highly beneficial when applying for a regular passenger flight. The GOBLEU instrument has currently booked its seats on a regular flight, operated daily at noon (e.g., ten round-trip flights between Tokyo Haneda Airport and Fukuoka Airport from 9:00 JST to 17:00 JST). If we select multiple flights in a day, GOBLEU could be a "frequent flyer" to identify the diurnal variations. As described in the previous section, all the security and safety inspection including X-ray test, radio interference checks and confirming with the airline that it will not cause any interference are required and confirmed for GOBLEU. However, operator training will be required to install each module safely onboard. After optimizing the FGHG, FNO2 and FSIP instrumental package, regular observations once per month were started in the spring of 2023. During the COVID-19 pandemic, the seats for instruments were easily bookable. However, after the pandemic, the regular passenger returns on their flight, and the instruments must book months in advance. In this operation chain, selecting a flight with fine weather is difficult. To overcome this, frequent flights with instruments are desirable with simple operation. Also, there are regular flights between Tokyo Haneda Airport and Fukuoka Airport less than every hour, from early morning to late night every day. In addition, GOBLEU should have a chance to elucidate diurnal

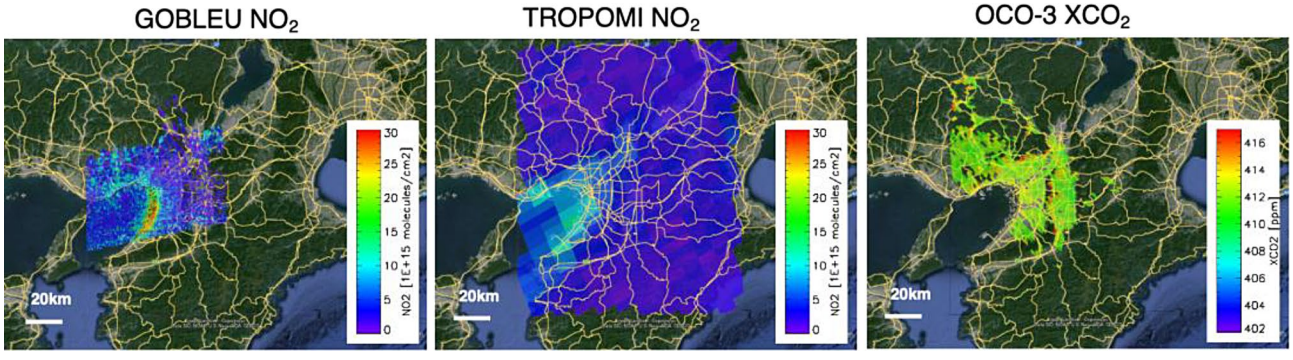

Fig. 12 GOBLEU, TROPOMI, and OCO-3 images over Osaka. Emission proxy NO_2 data over Osaka collected by GOBLEU NO_2 (left, 13:15 LT; UTC + 9), TROPOMI NO_2 (middle, 11:11 LT; UTC + 9), and OCO-3 CO_2 (right, 11:05 LT; UTC + 9). These observations were conducted on the same day (Oct. 27, 2020.) but at different times. GOBLEU data depict the local pattern of NO_2 concentration over Osaka. TROPOMI also suggests the high NO_2 concentration area near Osaka Bay, but it is difficult to identify the individual sources by pixel. OCO-3 also indicated a high CO_2 concentration area but did not correspond to the TROPOMI NO_2 map. These results also encourage the simultaneous observation of CO_2 and NO_2, to understand the emission sources well

variations and weekly dependent emission patterns with high-frequency observations.

As indicated in Fig. 5, ANA has a nationwide flight route network that connects key capital and major airports in Japan, such as Tokyo Haneda Airport and Hokkaido Wakkanai Airport, Tokyo Haneda Airport, and Kyushu Nagasaki Airport, which are potential destinations for future GOBLEU flights. These routes cover the high-intensity SIF, which indicates the production level (carbon removal) of the terrestrial biosphere area, such as the near-Sendai forestry area (see Fig. 5). The intensity of SIF indicates the strength of emission remover.

The area under the flight route Tokyo Haneda Airport to Fukuoka Airport includes approximately 30% of Japan's total CO_2 emissions and about 59% of Japan's Gross National Product (GDP) [69]. However, it is important to note that our airborne remote-sensing approach also shares the challenge due to cloud contamination. In the satellite observation case, around 80% of the data is cloud-contaminated despite the small foot-print size [70]. The data yield is expected to be impacted significantly in the summertime. In addition to anthropogenic CO_2 emissions, monitoring of natural CO_2 emissions and removals is a key to Japan's GHG management [71]. 67% of Japan's national land area is cover the forest [72].

Conclusion

Under the GOBLEU project, JAXA has developed a remote-sensing technique that can be operated on commercial passenger aircraft, by JAXA and ANAHD. The GOBLEU monitoring instrument suite is designed to collect CO_2, NO_2, and SIF data. The first trial flight with the NO_2 instrument was carried out and collected NO_2 data over major populated and industrialized areas. The NO_2 data showed timely snapshots of NO_2 spatial distributions, suggesting the utility of NO_2 data as a proxy for anthropogenic CO_2 emissions that should enhance emission estimations and attribution ability. GOBLEU instrument can be operated in almost any passenger aircraft without any modifications. While based on the same space-based observation technique as the current satellites, our airborne observation can collect denser and higher spatial resolution GHG data more frequently over key emission areas, such as Japanese megacities.

GOBLEU is a new challenge for GHG remote-sensing observation on a new platform and has the potential to open up a new field for passenger aircraft use. Nominally, passenger aircraft only carried passengers. To contribute to climate action by air company, the ANA Group is promoting ESG management that considers the Environment, Society, and Governance, aiming to realize a sustainable society and enhance corporate value. Under the slogan of "ANA Future Promise", the ANA group started actions to reduce the carbon emissions from aviation, actively adopting Sustainable Aviation Fuel (SAF) for aviation as well as a recycle-based society. In addition to these activities, ANAHD is scoping extended aviation use for climate mitigation activities such as climate monitoring tools.

GOBLEU aims to monitor the climate mitigation effort over Japan's intensive industrialized areas and contribute to the second GST scheduled in 2028. GOBLEU expects to provide timely GHG information by promptly collecting high-resolution GHG data and emission and removal estimates with greater information granularity. The high-spatial-resolution data should provide GHG information to stakeholders at different subnational levels (e.g., states/prefectures, cities, private sectors, and citizens) toward carbon neutrality under the Paris Climate Agreement. We also expect to expand the observation coverage overseas with domestic and international partnerships through enhancing internal cooperation.

Acknowledgements
The authors would like to thank Shin Ishida of JAXA and Kanako Hosokawa of Mitsubishi Electric Software Corporation for their support on re-processing. This study was conducted as part of the GOSAT data calibration activity. JAXA's GOSAT activities are funded by the Ministry of Education, Culture, Sports, Science and Technology, Japan.

Author contributions
HS and AK conceived the study. HS and SM developed the instrument. HS, AM, SM, AK, CH, FK, MS, YM, and YT collected the data. HS conducted the analysis supported by TO. HS and TO wrote the first manuscript based on all the authors' input. All the authors provided input, and reviewed and approved the final manuscript.

Funding
This research has been supported by the JAXA (Japan Aerospace Exploration Agency).

Data availability
All the data used in this manuscript are available from the following sources. EDGAR data: https://edgar.jrc.ec.europa.eu. OCO-3 data: https://www.earthdata.nasa.gov. The PM2.5 inventory data developed by MOE: https://www.env.go.jp/air/osen/pm/info.html. Soramame data: https://soramame.env.go.jp/download. TROPOMI NO_2 data: https://scihub.copernicus.eu. TROPOMI SIF data: https://climatesciences.jpl.nasa.gov/sif/. GOBLEU data supporting this study are available upon reasonable request. Please contact suto.hiroshi@jaxa.jp. Snapshot images of GOBLEU data are available from https://www.eorc.jaxa.jp/GOSAT/ANAexp/index_e.html.

Declarations

Competing interests
The authors declare no competing interests.

Author details
[1]Japan Aerospace Exploration Agency (JAXA), Tsukuba, Japan
[2]ANA Holdings Inc., Tokyo, Japan
[3]Earth from Space Institute, Universities Space Research Association (USRA), Columbia, MD, USA
[4]Department of Atmospheric and Oceanic Science, University of Maryland, College Park, MD, USA
[5]Graduate School of Engineering, Osaka University, Suita, Osaka, Japan
[6]JASTECS, Tokyo, Japan
[7]Remote Sensing Technology Center of Japan (RESTEC), Tokyo, Japan

Received: 29 October 2023 / Accepted: 8 August 2024
Published online: 16 August 2024

References

1. Secretariat UNFCCC. Technical dialogue of the first global stock take. Synthesis report by the co-facilitators on the technical dialogue. https://unfccc.int/documents/631600, 2023.
2. CEOS. CEOS and the UNFCCC Global Stocktake, https://ceos.org/gst/, 2021.
3. Kuze A, Suto H, Nakajima M, Hamazaki T. Thermal and near infrared sensor for carbon observation Fourier-transform spectrometer on the greenhouse gases observing Satellite for greenhouse gases monitoring. Appl Opt. 2009;48:6716–33. https://doi.org/10.1364/AO.48.006716.
4. Kuze A, Suto H, Shiomi K, Urabe T, Nakajima M, Yoshida J, Kawashima T, Yamamoto Y, Kataoka F, Buijs H. Level 1 algorithms for TANSO on GOSAT: processing and on-orbit calibrations. Atmos Meas Tech. 2012;5:2447–67. https://doi.org/10.5194/amt-5-2447-2012.
5. Kuze A, Suto H, Shiomi K, Kawakami S, Tanaka M, Ueda Y, Deguchi A, Yoshida J, Yamamoto Y, Kataoka F, Taylor TE, Buijs H. Update on GOSAT TANSO-FTS performance, operations, and data products after more than 6 years in space. Atmos Meas Tech. 2016;9:2445–61. https://doi.org/10.5194/amt-9-2445-2016.
6. Suto H, Kataoka F, Kikuchi N, Knuteson RO, Butz A, Haun M, Buijs H, Shiomi K, Imai H, Kuze A. Thermal and near-infrared sensor for carbon observation Fourier transform spectrometer-2 (TANSO-FTS-2) on the greenhouse gases observing SATellite-2 (GOSAT-2) during its first year in orbit. Atmos Meas Tech. 2021;14:2013–39. https://doi.org/10.5194/amt-14-2013-2021.
7. Suto H, Kataoka F, Knuteson RO, Shiomi K, Kikuchi N, Kuze A. Updated spectral radiance calibration on TIR bands for TANSO-FTS-2 onboard GOSAT-2, Atmos. Meas Tech. 2022;15:5399–413. https://doi.org/10.5194/amt-15-5399-2022.
8. Crisp D, Atlas RM, Breon F-M, Brown LR, Burrows JP, Ciais P, Connor BJ, Doney SC, Fung IY, Jacob DJ, Miller CE, O'Brien D, Pawson S, Randerson JT, Rayner P, Salawitch RJ, Sander SP, Sen B, Stephens GL, Tans PP, Toon GC, Wennberg PO, Wofsy SC, Yung YL, Kuang ZM, Chudasama B, Sprague G, Weiss B, Pollock R, Kenyon D, Schroll S. The Orbiting Carbon Observatory (OCO) Mission. Adv Space Res. 2004;34:700–9. https://doi.org/10.1016/j.asr.2003.08.062.
9. Crisp D, Miller CE, DeCola PL. NASA Orbiting Carbon Observatory: measuring the column averaged carbon dioxide mole fraction from space. J Appl Remote Sens. 2008;2:023508. https://doi.org/10.1117/1.2898457.
10. Crisp D, Pollock HR, Rosenberg R, Chapsky L, Lee RA, Oyafuso FA, Frankenberg C, O'Dell CW, Bruegge CJ, Doran GB, Eldering A. The on-orbit performance of the Orbiting Carbon Observatory-2 (OCO-2) instrument and its radiometrically calibrated products. Atmos Meas Tech. 2017;10:59–81. https://doi.org/10.5194/amt-10-59-2017.
11. Eldering A, Taylor TE, O'Dell CW, Pavlick R. The OCO-3 mission: measurement objectives and expected performance based on 1 year of simulated data. Atmos Meas Tech. 2019;12:2341–70. https://doi.org/10.5194/amt-12-2341-2019.
12. Hu H, Landgraf J, Detmers R, Borsdorff T, Aan de Brugh J, Aben I, Butz A, Hasekamp O. Toward global mapping of methane with TROPOMI: first results and Intersatellite comparison to GOSAT. Geophys Res Lett. 2018;45:3682–9. https://doi.org/10.1002/2018GL077259.
13. Matsunaga, Maksyutov, A GUIDEBOOK ON THE USE, OF SATELLITE GREENHOUSE GASES OBSERVATION DATA TO EVALUATE. AND IMPROVE GREENHOUSE GAS EMISSION INVENTORIES, 2018.
14. Byrne B, Baker DF, Basu S, Bertolacci M, Bowman KW, Carroll D, Chatterjee A, Chevallier F, Ciais P, Cressie N, Crisp D, Crowell S, Deng F, Deng Z, Deutscher NM, Dubey MK, Feng S, García OE, Herkommer B, Hu L, Jacobson AR, Janardanan R, Jeong S, Johnson MS, Jones DBA, Kivi R, Liu J, Liu Z, Maksyutov S, Miller JB, Miller SM, Morino I, Notholt J, Oda T, O'Dell CW, Oh Y-S, Ohyama H, Patra PK, Peiro H, Petri C, Philip S, Pollard DF, Poulter B, Remaud M, Schuh A, Sha MK, Shiomi K, Strong K, Sweeney C, Té Y, Tian H, Velazco VA, Vrekoussis M, Warneke T, Worden JR, Wunch D, Yao Y, Yun J, Zammit-Mangion A, Zeng N. National CO_2 budgets (2015–2020) inferred from atmospheric CO_2 observations in support of the global stocktake. Earth Syst Sci Data. 2023;15:963–1004. https://doi.org/10.5194/essd-15-963-2023.
15. Worden JR, Cusworth DH, Qu Z, Yin Y, Zhang Y, Bloom AA, Ma S, Byrne BK, Scarpelli T, Maasakkers JD, Crisp D, Duren R, Jacob DJ. The 2019 methane budget and uncertainties at 1° resolution and each country through bayesian integration of GOSAT total column methane data and a priori inventory estimates. Atmos Chem Phys. 2022;22:6811–41. https://doi.org/10.5194/acp-22-6811-2022.
16. ICAO, Economic Development- Air Transport Bureau, Effects of Novel Coronavirus (COVID-19) on Civil Aviation: Economic Impact Analysis. 2022. https://www.icao.int/sustainability/Documents/Covid-19/ICAO_coronavirus_Econ_Impact.pdf
17. ICAO, Economic impact https://www.icao.int/Newsroom/Pages/2020-passenger-totals-drop-60-percent-as-COVID19-assault-on-international-mobility-continues.aspx, 2021.
18. Gerlein-Safdi C, Keppel-Aleks G, Wang F, Frolking S, Mauzerall DL. Satellite monitoring of natural reforestation efforts in China's drylands. One Earth. 2020;2(1):98–108. https://doi.org/10.1016/j.oneear.2019.12.015.
19. Anema JCS, Boersma KF, Stammes P, Koren G, Woodgate W, Köhler P, Frankenberg C, Stol J. Monitoring the impact of forest changes on carbon uptake with solar-induced fluorescence measurements from GOME-2A and TROPOMI for an Australian and Chinese case study. Biogeosciences. 2024;21:2297–311. https://doi.org/10.5194/bg-21-2297-2024.
20. Hirabayashi T. 2020. Contribution of JAXA's Earth Observation Missions to Water Cycle and Climate Studies, Disaster Mitigation, and Operational Applications, EGU General Assembly 2020, EGU2020-19165. https://doi.org/10.5194/egusphere-egu2020-19165, 2020.
21. Sierk B, Bézy JL, Löscher A, Meijer Y. 2019. The European CO_2 Monitoring Mission: observing anthropogenic greenhouse gas emissions from space, International Conference on Space Optics - ICSO 2018; 111800M. https://doi.org/10.1117/12.2535941, 2019.
22. Hakkarainen J, Szelag ME, Ialongo I, Retscher C, Oda T. and D., Crisp (2021), Analyzing nitrogen oxides to carbon dioxide emission ratios from space: A case study of Matimba Power Station in South Africa, Atmos. Env., X, https://doi.org/10.1016/j.aeaoa.2021.100110, 2021.
23. Hakkarainen J, Ialongo I, Oda T, Szelag ME, O'Dell CW, Eldering A, Crisp D. Building a bridge: characterizing major anthropogenic point sources in the South African Highveld region using OCO-3 carbon dioxide snapshot area maps and Sentinel-5P/TROPOMI nitrogen dioxide columns. Environ Res Lett. 2023;18(035003). https://doi.org/10.1088/1748-9326/acb837.
24. Fujinawa T, Kuze A, Suto H, Shiomi K, Kanaya Y, Kawashima T et al. (2021). First concurrent observations of NO_2 and CO_2 from power plant plumes by airborne remote sensing. Geophysical Research Letters, 48, e2021GL092685. https://doi.org/10.1029/2021GL092685, 2021.
25. Reuter M, Buchwitz M, Schneising O, Krautwurst S, O'Dell CW, Richter A, Bovensmann H, Burrows JP. Towards monitoring localized CO_2 emissions from space: co-located regional CO_2 and NO_2 enhancements observed by the OCO-2 and S5P satellites. Atmos Chem Phys. 2019;19:9371–83. https://doi.org/10.5194/acp-19-9371-2019.
26. Lei R, Feng S, Xu Y, Tran S, Ramonet M, Grutter M, Garcia A, Campos-Pineda M, Lauvaux T. Reconciliation of asynchronous satellite-based NO_2 and XCO_2 enhancements with mesoscale modeling over two urban landscapes. Remote Sens Environ. 2022;281:113241. https://doi.org/10.1016/j.rse.2022.113241. .
27. Platt U. and J.Stutz, Differential Optical absorption spectroscopy, principles and applications. Springer; 2008.
28. Frankenberg C, Platt U, Wagner T. Iterative maximum a posteriori (IMAP)-DOAS for retrieval of strongly absorbing trace gases: Model studies for CH_4 and CO_2 retrieval from near infrared spectra of SCIAMACHY onboard ENVISAT, Atmos. Chem. Phys., 5, 9–22, 2005 www.atmos-chem-phys.org/acp/5/9/, 2005.
29. Butz A, Guerlet S, Hasekamp O, Schepers D, Galli A, Aben I, Frankenberg C, Hartmann J-M, Tran H, Kuze A, Keppel-Aleks G, Toon G, Wunch D, Wennberg P, Deutscher N, Griffith D, Macatangay R, Messerschmidt J, Notholt J, Warneke T. Toward accurate CO_2 and CH_4 observations from GOSAT. Geophys Res Lett. 2011;38:L14812. https://doi.org/10.1029/2011GL047888.
30. Butz A, Guerlet S, Hasekamp OP, Kuze A, Suto H. Using ocean-glint scattered sunlight as a diagnostic tool for satellite remote sensing of greenhouse gases. Atmos Meas Tech. 2013;6:2509–20. https://doi.org/10.5194/amt-6-2509-2013.
31. Crisp D, Fisher BM, O'Dell C, Frankenberg C, Basilio R, Bösch H, Brown LR, Castano R, Connor B, Deutscher NM, Eldering A, Griffith D, Gunson M, Kuze A, Man- drake L, McDuffie J, Messerschmidt J, Miller CE, Morino I, Natraj V, Notholt J, O'Brien DM, Oyafuso F, Polonsky I, Robinson J, Salawitch R, Sherlock V, Smyth M, Suto H, Taylor TE, Thompson DR, Wennberg PO, Wunch D, Yung YL. The ACOS CO_2 retrieval algorithm – part II: GlobalXCO2 datacharacterization,Atmos.Meas.Tech.,5,687– 707, https://doi.org/10.5194/amt-5-687-2012, 2012.

32. Heymann J, Reuter M, Hilker M, Buchwitz M, Schneising O, Bovensmann H, Burrows JP, Kuze A, Suto H, Deutscher NM, Dubey MK, Griffith DWT, Hase F, Kawakami S, Kivi R, Morino I, Petri C, Roehl C, Schneider M, Sher- lock, Sussmann V, Velazco R, Warneke VA, T., and, Wunch D. Consistent satellite XCO_2 retrievals from SCIAMACHY and GOSAT using the BESD algorithm, Atmos. Meas. Tech., 8, 2961–2980, https://doi.org/10.5194/amt-8-2961-2015, 2015.
33. O'Dell CW, Connor B, Bösch H, O'Brien D, Frankenberg C, Castano R, Christi M, Eldering D, Fisher B, Gunson M, McDuffie J, Miller CE, Natraj V, Oyafuso F, Polonsky I, Smyth M, Taylor T, Toon GC, Wennberg PO, Wunch D. The ACOS CO_2 retrieval algorithm – part 1: description and validation against synthetic observations. Atmos Meas Tech. 2012;5:99–121. https://doi.org/10.5194/amt-5-99-2012.
34. Yoshida Y, Ota Y, Eguchi N, Kikuchi N, Nobuta K, Tran H, Morino I, Yokota T. Retrieval algorithm for CO_2 and CH_4 column abundances from short-wavelength infrared spec- tral observations by the greenhouse gases observing satellite. Atmos Meas Tech. 2011;4:717–34. https://doi.org/10.5194/amt-4-717-2011.
35. Kikuchi N, Yoshida Y, Uchino O, Morino I, Yokota T. An advanced retrieval algorithm for greenhouse gases using polar- ization information measured by GOSAT TANSO-FTS SWIR I: Simulation study. J Geophys Res -Atmos. 2016;121:13129–57. https://doi.org/10.1002/2015JD024720.
36. Noël S, Reuter M, Buchwitz M, Borchardt J, Hilker M, Bovensmann H, Burrows JP, Di Noia A, Suto H, Yoshida Y, Buschmann M, Deutscher NM, Feist DG, Griffith DWT, Hase F, Kivi R, Morino I, Notholt J, Ohyama H, Petri C, Podolske JR, Pollard DF, Sha MK, Shiomi K, Sussmann R, Té Y, Velazco VA, Warneke T. XCO_2 retrieval for GOSAT and GOSAT-2 based on the FOCAL algorithm. Atmos Meas Tech. 2021;14:3837–69. https://doi.org/10.5194/amt-14-3837-2021.
37. Noël S, Reuter M, Buchwitz M, Borchardt J, Hilker M, Schneising O, Bovensmann H, Burrows JP, Di Noia A, Parker RJ, Suto H, Yoshida Y, Buschmann M, Deutscher NM, Feist DG, Griffith DWT, Hase F, Kivi R, Liu C, Morino I, Notholt J, Oh Y-S, Ohyama H, Petri C, Pollard DF, Rettinger M, Roehl C, Rousogenous C, Sha MK, Shiomi K, Strong K, Sussmann R, Té Y, Velazco VA, Vrekoussis M, Warneke T. Retrieval of greenhouse gases from GOSAT and GOSAT-2 using the FOCAL algorithm. Atmos Meas Tech. 2022;15:3401–37. https://doi.org/10.5194/amt-15-3401-2022.
38. Fayt C, Danckaert T, Van Roozendael M. May : QDOAS software user manual 2.111, BIRA-IASB, Uccle, Belgium, http://uv-vis.aeronomie.be/software/QDOAS/QDOAS_manual.pdf (last access: 10 2017), 2016.
39. Frankenberg C, Berry J. Solar Induced Chlorophyll Fluorescence: Origins, Relation to Photosynthesis and Retrieval. https://doi.org/10.1016/B978-0-12-409548-9.10632-3, 2017.
40. Frankenberg C, Butz A, Toon GC. Disentangling chlorophyll fluorescence from atmospheric scattering effects in O2 A-band spectra of reflected sun-light. Geophys Res Lett. 2011a;38:L03801. https://doi.org/10.1029/2010GL045896.
41. Frankenberg C, Fisher JB, Worden J, Badgley G, Saatchi SS, Lee J-E, Toon GC, Butz A, Jung M, Kuze A, Yokota T. New global observations of the terrestrial carbon cycle from GOSAT: patterns of plant fluorescence with gross primary productivity. Geophys Res Lett. 2011b;38:L17706. https://doi.org/10.1029/2011GL048738.
42. Guanter L, Frankenberg C, Dudhia A, Lewis PE, Gomez-Dans J, Kuze A, Suto H, Grainger RG. Retrieval and global assessment of terrestrial chlorophyll fluorescence from GOSAT apace measurements. Remote Sens Envir. 2012;121:236–51. https://doi.org/10.1016/j.rse.2012.02.006.
43. Joiner J, Yoshida Y, Vasilkov AP, Middleton EM, Camp- bell PKE, Yoshida Y, Kuze A, Corp LA. Filling-in of near-infrared solar lines by terrestrial fluorescence and other geo- physical effects: simulations and space-based observations from SCIAMACHY and GOSAT. Atmos Meas Tech. 2012;5:809–29. https://doi.org/10.5194/amt-5-809-2012.
44. Frankenberg C, O'Dell C, Guanter L, McDuffie J. Remote sensing of near-infrared chlorophyll fluorescence from space in scattering atmospheres: implications for its retrieval and interferences with atmospheric CO_2 retrievals. Atmos Meas Tech. 2012;5:2081–94. https://doi.org/10.5194/amt-5-2081-2012.
45. Joiner J, Guanter L, Lindstrot R, Voigt M, Vasilkov AP, Middleton EM, Huemmrich KF, Yoshida Y, Frankenberg C. Global monitoring of terrestrial chlorophyll fluorescence from moderate-spectral-resolution near-infrared satellite measurements: methodology, simulations, and application to GOME-2, Atmos. Meas Tech. 2013;6:2803–23. https://doi.org/10.5194/amt-6-2803-2013.
46. Joiner J, Yoshida Y, Vasilkov AP, Yoshida Y, Corp LA, Middleton EM. First observations of global and seasonal terrestrial chlorophyll fluorescence from space. Biogeosciences. 2011;8:637–51. https://doi.org/10.5194/bg-8-637-2011.
47. Guanter L, Aben I, Tol P, Krijger JM, Hollstein A, Köhler P, Damm A, Joiner J, Frankenberg C, Landgraf J. Potential of the TROPOspheric monitoring instrument (TROPOMI) onboard the Sentinel-5 precursor for the monitoring of terrestrial chlorophyll fluorescence. Atmos Meas Tech. 2015;8:1337–52. https://doi.org/10.5194/amt-8-1337-2015.
48. Taylor TE, O'Dell CW, Baker D, Bruegge C, Chang A, Chapsky L, Chatterjee A, Cheng C, Chevallier F, Crisp D, Dang L, Drouin B, Eldering A, Feng L, Fisher B, Fu D, Gunson M, Haemmerle V, Keller GR, Kiel M, Kuai L, Kurosu T, Lambert A, Laughner J, Lee R, Liu J, Mandrake L, Marchetti Y, McGarragh G, Merrelli A, Nelson RR, Osterman G, Oyafuso F, Palmer PI, Payne VH, Rosenberg R, Somkuti P, Spiers G, To C, Weir B, Wennberg PO, Yu S, Zong J. Evaluating the consistency between OCO-2 and OCO-3 XCO_2 estimates derived from the NASA ACOS version 10 retrieval algorithm. Atmos Meas Tech. 2023;16:3173–209. https://doi.org/10.5194/amt-16-3173-2023.
49. Cusworth DH, Duren RM, Thorpe AK, Eastwood ML, Green RO, Dennison PE, et al. Quantifying global power plant carbon dioxide emissions with imaging spectroscopy. AGU Adv. 2021;2(e2020AV000350). https://doi.org/10.1029/2020AV000350.
50. Crippa M, Oreggioni G, Guizzardi D, Muntean M, Schaaf E, Lo Vullo E, Solazzo E, Monforti-Ferrario F, Olivier JGJ, Vignati E. Fossil CO_2 and GHG emissions of all world countries – 2019 Report, EUR 29849 EN, Publications Office of the European Union, Luxembourg, 2019, ISBN 978-92-76-11100-9, https://doi.org/10.2760/687800, JRC117610, 2020a.
51. Crippa M, Solazzo E, Huang G, Guizzardi D, Koffi E, Muntena M, Schieberle C, Friedrick R, Janssens- Maenhout G. High resolution temporal profiles in the emissions Database for Global Atmospheric Research. Sci Data. 2020b;7:121. https://doi.org/10.1038/s41597-020-0462-2.
52. Crippa M, Oreggioni G, Guizzardi D, Muntean M, Schaaf E, Lo Vullo E, Solazzo E, Monforti-Ferrario F, Olivier JGJ, Vignati E. EDGAR v5.0 Greenhouse Gas Emissions, https://data.europa.eu/doi/10.2904/JRC_ DATASET_EDGAR (last access: 12 April 2020), 2020.
53. Köhler P, Behrenfeld MJ, Landgraf J, Joiner J, Magney TS, Frankenberg C. Global retrievals of solar-induced chlorophyll fluorescence at red wavelengths with TROPOMI. Geophys Res Lett. 2020;47:e2020GL087541. https://doi.org/10.1029/2020GL087541.
54. Chance K, Kurucz RL. An improved high-resolution solar reference spectrum for earth's atmosphere measurements in the ul- traviolet, visible, and near infrared. J Quant Spectrosc Radiative Transf. 2010;111(9):1289–95.
55. Spurr R, Christi MJ. Linearization of the Interaction Principle: Analytic jacobians in the Radiant Model. J Quant Spectrosc Radiat Transf. 2006;103/3:431–46. https://doi.org/10.1016/j.jqsrt.2006.05.001.
56. Miyazaki K, Chemical Reanalysis TROPESS. NO_2 Monthly 3-dimensional Product V1, Greenbelt, MD, USA, Goddard Earth Sciences Data and Information Services Center (GES DISC), Accessed: [Data Access Date], https://doi.org/10.5067/F4FE5VWM9501., 2024.
57. Tilstra LG, de Graaf M, Trees VJH, Litvinov P, Dubovik O, Stammes P. A directional surface reflectance climatology determined from TROPOMI observations. Atmos Meas Tech. 2024;17:2235–56. https://doi.org/10.5194/amt-17-2235-2024.
58. van Geffen J, Eskes H, Compernolle S, Pinardi G, Verhoelst T, Lambert J-C, Sneep M, ter Linden M, Ludewig A, Boersma KF, Veefkind JP. Sentinel-5P TROPOMI NO_2 retrieval: impact of version v2.2 improvements and comparisons with OMI and ground-based data. Atmos Meas Tech. 2022;15:2037–60. https://doi.org/10.5194/amt-15-2037-2022.
59. Boersma KF, Eskes HJ, Brinksma EJ. Error analysis for tropospheric NO_2 retrieval from space. J Geophys Res. 2004;109:D04311. https://doi.org/10.1029/2003JD003962.
60. Veefkind JP, Aben I, McMullan K, Förster H, de Vries J, Otter G, et al. TROPOMI on the ESA Sentinel-5 precursor: a GMES mission for global observations of the atmospheric composition for climate, air quality and ozone layer applications. Remote Sens Environ. 2012;120:70–83. https://doi.org/10.1016/j.rse.2011.09.027.
61. Riess TCVW, Boersma KF, Van Roy W, de Laat J, Dammers E, van Vliet J. To new heights by flying low: comparison of aircraft vertical NO_2 profiles to model simulations and implications for TROPOMI NO_2 retrievals. Atmos Meas Tech. 2023;16:5287–304. https://doi.org/10.5194/amt-16-5287-2023.
62. Formulation Committee for PM2.5 Emission Inventory and, Profile S. PM2.5 Emission Inventory and Source Profile, 2019, (in Japanese), https://www.env.go.jp/air/osen/pm/info.html#INVENTORY, 2019.
63. Hersbach H, Bell B, Berrisford P, Biavati G, Horányi A, Muñoz Sabater J, Nicolas J, Peubey C, Radu R, Rozum I, Schepers D, Simmons A, Soci C, Dee D, Thépaut J-N. (2023): ERA5 hourly data on single levels from 1940 to present.

Copernicus Climate Change Service (C3S) Climate Data Store (CDS), https://doi.org/10.24381/cds.adbb2d47 (Accessed on 25-Jul-2024).
64. Boersma KF, Jacob DJ, Trainic M, Rudich Y, DeSmedt I, Dirksen R, Eskes HJ. Validation of urban NO_2 concentrations and their diurnal and seasonal variations observed from the SCIAMACHY and OMI sensors using in situ surface measurements in Israeli cities. Atmos Chem Phys. 2009;9:3867–79. https://doi.org/10.5194/acp-9-3867-2009.
65. Wunch D, Toon GC, Blavier J-FL, Washenfelder RA, Notholt J, Connor BJ, Griffith DWT, Sherlock V, Wennberg PO. The total Carbon Column Observing Network. Philosophical Trans Royal Soc A: Math Phys Eng Sci. 2011;369. https://doi.org/10.1098/rsta.2010.0240.
66. Frey M, Sha MK, Hase F, Kiel M, Blumenstock T, Harig R, Surawicz G, Deutscher NM, Shiomi K, Franklin JE, Bösch H, Chen J, Grutter M, Ohyama H, Sun Y, Butz A, Mengistu Tsidu G, Ene D, Wunch D, Cao Z, Garcia O, Ramonet M, Vogel F, Orphal J. Building the COllaborative Carbon Column Observing Network (COCCON): long-term stability and ensemble performance of the EM27/SUN Fourier transform spectrometer. Atmos Meas Tech. 2019;12:1513–30. https://doi.org/10.5194/amt-12-1513-2019.
67. Herman J, Abuhassan N, Kim J, Kim J, Dubey M, Raponi M, Tzortziou M. Underestimation of column NO_2amounts from the OMI satellite compared to diurnally varying ground-based retrievals from multiple PANDORA spectrometer instruments. Atmos Meas Tech. 2019;12:5593–612. https://doi.org/10.5194/amt-12-5593-2019.
68. Kim S, Kim D, Hong H, Chang L-S, Lee H, Kim D-R, Kim D, Yu J-A, Lee D, Jeong U, Song C-K, Kim S-W, Park SS, Kim J, Hanisco TF, Park J, Choi W, Lee K. First-time comparison between NO_2 vertical columns from Geostationary Environmental Monitoring Spectrometer (GEMS) and Pandora measurements. Atmos Meas Tech. 2023;16:3959–72. https://doi.org/10.5194/amt-16-3959-2023.
69. CAO. https://www.esri.cao.go.jp/jp/sna/menu.html, 2022.
70. Miller CE, Crisp D, DeCola PL, Olsen SC, Randerson JT, Michalak AM, Alkhaled A, Rayner P, Jacob DJ, Suntharalingam P, Jones DBA, Denning AS, Nicholls ME, Doney SC, Pawson S, Boesch H, Connor BJ, Fung IY, O'Brien D, Salawitch RJ, Sander SP, Sen B, Tans P, Toon GC, Wennberg PO, Wofsy SC, Yung YL. Law, R. M.; Precision requirements for space-based XCO2 data, J. Geophys. Res., 112, D10314, https://doi.org/10.1029/2006JD007659, 2007.
71. Japan's Nationally Determined Contribution (NDC). https://unfccc.int/sites/default/files/NDC/2022-06/JAPAN_FIRST%20NDC%20%28UPDATED%20SUBMISSION%29.pdf
72. Forestry, Agency. Ministry of Agriculture, Forestry and Fisheries, Japan, Annual reports on Forest and Forestry in Japan Fiscal Year 2021; https://www.maff.go.jp/e/data/publish/attach/pdf/index-96.pdf, 2021.

Publisher's Note